

Received March 28, 2022, accepted April 20, 2022, date of publication May 9, 2022, date of current version May 18, 2022.

Digital Object Identifier 10.1109/ACCESS.2022.3173325

Torque Ripple Reduction for BLDC Permanent Magnet Motor Drive Using DC-Link Voltage and Current Modulation

CHING-LON HUANG¹, (Student Member, IEEE), FENG-CHI LEE², CHIA-JUNG LIU²,
JYUN-YOU CHEN¹, (Student Member, IEEE), YI-JEN LIN¹, (Graduate Student Member, IEEE),
AND SHIH-CHIN YANG¹, (Senior Member, IEEE)

¹Department of Mechanical Engineering, National Taiwan University, Taipei 106319, Taiwan

²Industrial Technology Research Institute, Hsinchu 310401, Taiwan

Corresponding author: Shih-Chin Yang (scy99@ntu.edu.tw)

This work was supported in part by the Mechanical and Mechatronics Systems Laboratory of Industrial Technology Research Institute under Grant K453RE1500, and in part by the Taiwanese Ministry of Science and Technology under Grant 09HT512031.

ABSTRACT This paper proposes a torque ripple reduction for brushless DC (BLDC) permanent magnetic (PM) motor drive based on the DC-link voltage pulse amplitude modulation (PAM). The proposed method improves torque ripple drawback for BLDC drives at low speed. BLDC drives have the better inverter efficiency and requires low position sensing resolution. However, both freewheeling current during diode conduction and discontinuous motor phase current cause high torque ripples. In this paper, a front-end DC converter is added to improve BLDC torque ripples. Although the integration of DC converter and BLDC drive has been reported, the DC voltage regulation for the BLDC torque ripple compensation is this paper novelty. On the basis, the DC bus is modulated during diode conduction to manipulate the DC current dynamically every BLDC commutation period. In addition considering the discontinuous six-step commutation, the DC current is also regulated with the 6th-order spatial harmonic to minimize the commutation reflected torque ripple. The proposed torque ripple compensation of BLDC drive is verified by simulation for different PM motor types. According to experimental results, around 40% torque ripple reduction on a PM motor is demonstrated using the proposed BLDC drive with DC voltage modulation.


INDEX TERMS Torque ripple, brushless DC motor, and pulse amplitude modulation.

I. INTRODUCTION

BLDC drive has the advantages of better inverter efficiency and requires low position sensing resolution. For certain motion applications such as electric bikes and converter belt, standard BLDC drives have issues on high torque ripples especially at low speed [1]. The main results causing torque ripples are the diode freewheeling current every commutation switch. In this case, motor current spikes are resultant leading to misalignment between desired and actual currents [2].

In order to reduce BLDC reflected torque ripples, several BLDC control methods have been proposed. [3] manipulates three-phase PWM switching patterns during the commutation period to reduce the torque ripple. During the diode conduction period, the chop mode is implemented on both

inverter high-side and low-side switch. PWM_ON_PWM [4], ON_PWM [5], and PWM_ON [6] related PWM drive techniques are proposed for torque ripple reduction. In these cases, the PWM duty is adjusted to create an overlap period for the same rising and falling current within diode conduction. However, these methods require various operation modes dependent on different PWM duties. Different from prior PWM modification, [7] adds a hysteresis current control for the DC-link current regulation during the diode conduction. However, the PWM modification is still implemented for ripple reduction. Other side effects, e.g. efficiency and reliability, might induce due to additional switches among different PWM duties. Instead of BLDC six-step commutation, [8] uses space vector PWM (SVPWM) to drive the PM motor with trapezoidal EMF. By adjusting dq current vector commands, the trapezoidal EMF reflected torque ripples are compensated.

The associate editor coordinating the review of this manuscript and approving it for publication was Shaopeng Wu .

Different from PWM modification, the DC-link voltage modulation is also proposed for the improvement on BLDC torque ripples. The DC-link voltage modulation, also called pulse amplitude modulation (PAM) has the advantages of better motor efficiency comparing to PWM BLDC [9] and SVPWM BLDC [10]. [11] proposes a torque ripple reduction through the DC-link voltage regulation. On this basis, the DC-link voltage is increased to remain constant motor currents during normal BLDC commutation. [12] realizes the inverter topology in [11] by adding dual voltage supply converter at front-end stage. Multiple switches are designed between every two different voltage levels. However, only freewheeling diode conduction is taken into consideration. For BLDC drive under discontinuous six-step commutation, the misalignment between the trapezoidal current and sinusoidal electromotive force (EMF) voltage causes additional torque harmonics. At this time, no ripple compensation method is reported to improve this current and EMF misalignment issue.

Torque ripple can also be reduced through current regulation. [13] adjusts the current command with the high-performance current controller to reduce torque ripple. Although the current control method is based on Field Oriented Control (FOC) drive, this pre-process command and regulation can be implemented on DC voltage or DC current for BLDC drive ripple reduction [14]. However, the control bandwidth must be sufficiently high for the manipulation of both DC voltage and current. Considering the DC voltage regulation, the front-end DC converter with wide-bandgap switches can be implemented for high bandwidth voltage control. [15] proposes the concept of DC voltage regulation to increase FOC drive efficiency specifically for the control using space vector PWM (SVPWM).

This paper proposes a torque ripple reduction for BLDC drive based on the PAM control of DC-link voltage. The proposed BLDC drive contains a front-end buck converter and LC filter to realize DC voltage modulation. The DC-link voltage is regulated dependent on six-step commutation conditions. Six-step commutation issues are considered on both diode conduction period and non-orthogonal relation between trapezoidal current and sinusoidal magnet flux. In order to achieve high dynamic DC voltage regulation, a cascaded current and voltage controller is implemented to compensate the converter filter reflected resonance. After that, the dynamic model of inverter freewheeling during diode conduction is developed for the DC voltage modulation. Besides considering the influence of discontinuous trapezoidal current, the DC voltage is regulated dependent on rotor position to reduce torque ripple. The proposed BLDC drive for torque ripple reduction is verified by simulations for PM motors with sinusoidal and trapezoidal EMF voltages. A PM motor with sinusoidal EMF is selected for experimental evaluation. It is concluded that around 40% torque ripple reduction is achieved using the proposed BLDC drive.

TABLE 1. Comparison of torque ripple reduction.

Paper	Inverter structure	PWM METHOD	Ripple compensation	Performance
[8]	Six-leg inverter	SVPWM	1.Offline model 2.Feedforward control	No data is presented
[4]	Six-leg inverter	PWM BLDC	1.Inverter model 2.Switching duty control	13.5% ripple improvement (Various modes)
[12]	Six-leg inverter + two SEPIC converters	PAM BLDC	1.Inverter model 2.Two-level voltage control	28.9% ripple improvement
Proposed method	Six-leg inverter + one buck converter	PAM BLDC	1.Motor and inverter model 2.Adjustable voltage control	40.0% ripple improvement

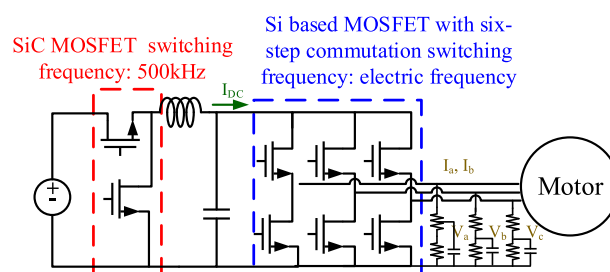


FIGURE 1. Proposed PAM BLDC drive and sensing device with front-end buck converter.

II. RIPPLE COMPENSATION METHODS COMPARISON

This section compares state-of-the-art torque ripple compensation for BLDC drives. Table 1 lists the specification of different torque ripple compensation methods. Both [8] and [4] realize the ripple compensation based on existing six-leg inverter. Although no additional hardware is required, the saturation at high voltage duty and complicated control algorithm are primarily challenge. By contrast, [12] adds two SEPIC converters to minimize the diode conduction current. This paper simplifies the hardware in [12] by a simple two-switch buck converter. Besides diode conduction, the misalignment between sinusoidal EMF and trapezoidal BLDC current is also considered. The compensation performance is improved to 40.0% through the dynamic DC voltage regulation.

III. PROPOSED DC VOLTAGE MODULATION

This section proposes the BLDC drive with front-end buck converter for torque ripple reduction. Fig. 1 shows this PAM BLDC drive topology. A front-end buck converter with SiC MOSFET is designed to allow 500kHz switch frequency for high dynamic voltage control, The Si based six-leg inverter is still maintained for BLDC commutation. This drive enables DC-link voltage V_{DC} to be manipulated based on the desired voltage command. To remove PWM harmonics caused by SiC buck converter, an inductor and capacitor are used to formulate the LC filter.

using DC-link voltage feedback signal. First, (3) shows a voltage controller $G_{vc}(s)$. The controller pole is designed to cancel the zero of transfer function in (2) while the control zero decouples the resonant pole in (2). Besides, an integral gain K_{i_v} is to remove steady state error. Under this effect, $G_{vc}(s)$ can be developed by

$$G_{vc}(s) = K_{p_v} \frac{s + zero}{s + pole} + \frac{K_{i_v}}{s} = K_{p_v} \frac{s + f_{res}}{s + R_s/L_s} + \frac{K_{i_v}}{s} \quad (3)$$

where K_{p_v} and K_{i_v} are the proportional and integral gain of voltage controller, and is the corresponding resonance frequency. By applying pole/zero cancellation from (3) to (2), the frequency response of $V_{DC}(s)/V_{DC}^*(s)$ is changed by the blue dash line in Fig. 3. It is seen that the resonance is reduced while the modulation bandwidth is increased from 500Hz to 1700Hz. In this analysis, the bandwidth of the voltage control system is determined by -3dB gain. Besides due to the high bandwidth feedback control, the proposed voltage controller has the ability to withstand at least 50% parameter error of the inductance.

C. CURRENT FEEDBACK CONSIDERING FREEWHEELING EFFECT:

The current closed-loop controller in Fig. 2 is key to manipulate the DC-link voltage command V_{DC}^* for torque ripple reduction. Traditional PAM BLDC directly measures the DC-link current for regulation [18]. However considering the diode conduction, the freewheeling current flows through motor windings even when DC current is zero. In this case, the freewheeling reflected current should be considered for the current regulation to compensate torque ripples.

To compensate this freewheeling current reflected ripple, an improved current regulation is proposed through direct phase current measurement. On the basis, the equivalent total motor current instead of DC current is reconstructed based on Table 3. In this table, the equivalent total current is equal to a specific phase current at different rotor positions. During the diode conduction, the unchanged phase current is selected as the equivalent total current for the current control in Fig. 2.

Fig. 4(a) illustrates A-phase (a) terminal voltage and (b) current during the six-step commutation within one electric period. As seen from the commutation stage V6 between $5\pi/3-2\pi$, the BLDC commutation contains both diode conduction and normal conduction sub-period. Fig. 5 further explains three-phase inverter currents during V6 period in Fig. 4. In (a), the diode conduction sub-period in V6 is shown. At this instant, the inverter current flows across from C-phase to both B-phase switch and A-phase body diode. After a certain time, the freewheeling current in A-phase disappears and the commutation period changes to the normal BLDC commutation in (b). It is noted that in (a), the DC-link current I_{DC} is not equal to the total current across motor for torque production because of freewheeling in I_A . More importantly, the equivalent effective total current can be obtained with the

TABLE 3. Total current feedback table.

Electric position	Sector	Phase A	Phase B	Phase C	Equivalent total current
0–30	1	In	Out	×	-B
30–60					+A
60–90	2	In	×	Out	-C
90–120					+B
120–150	3	×	In	Out	-A
150–180					+C
180–210	4	Out	In	×	-B
210–240					+A
240–270	5	Out	×	In	-C
270–300					+B
300–330	6	×	Out	In	-A
330–360					+C

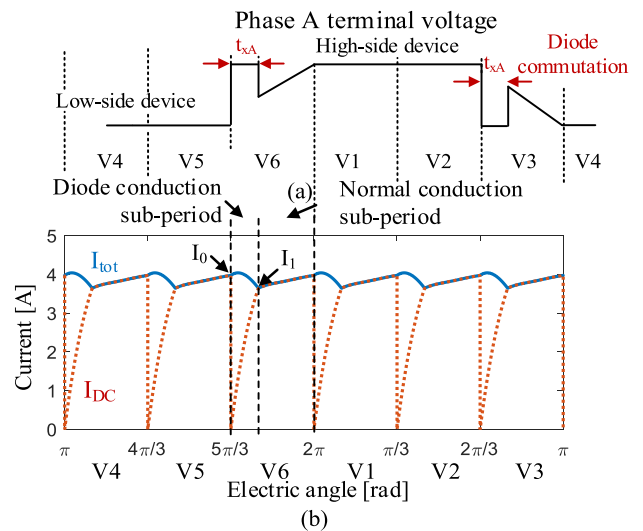


FIGURE 4. Illustration of A-phase (a) terminal voltage and (b) current under BLDC drive (PAM control without PWM phase voltage is assumed).

knowledge of three-phase currents. For instance, considering the diode conduction in V6 case at the position of $5\pi/3$, the total current flows across C-phase high-side. According to Table 3, the equivalent total current is the same as positive C-phase current.

Fig. 4(b) compares the measured DC-link current I_{DC} and proposed equivalent total current I_{tot} with respect to the rotor position. In this figure, I_{tot} is calculated based on the phase current selection in Table 3. By using the proposed I_{tot} for current control, it is expected that current feedback I_{tot} contains freewheeling reflected current for the following torque ripple compensation development.

Fig. 4(b) compares the measured DC-link current I_{DC} and proposed equivalent total current I_{tot} with respect to the rotor position. In this figure, I_{tot} is calculated based on the phase current selection in Table 3. By using the proposed I_{tot} for current control, it is expected that current feedback I_{tot} contains

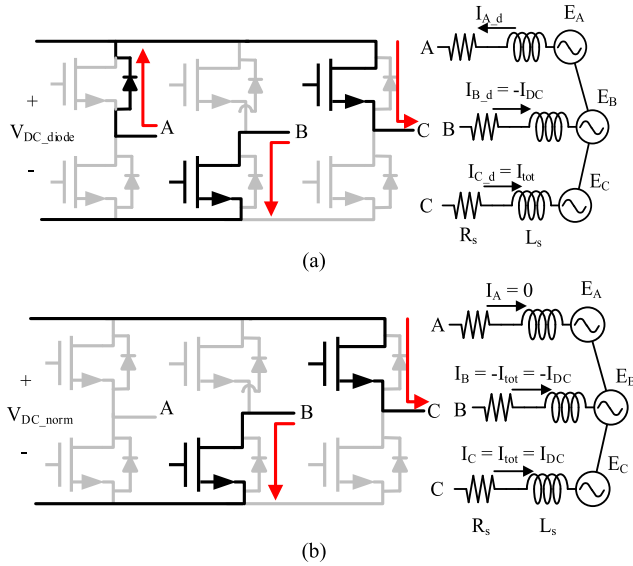


FIGURE 5. Illustration of three-phase currents during BLDC commutation V6 period in Fig. 4: (a) diode conduction sub-period (b) normal commutation sub-period.

the freewheeling reflected current for the following torque ripple compensation development.

D. CURRENT CONTROL WITH FEEDFORWARD:

The sufficient current control bandwidth is also required to dynamically modulate the total current for the BLDC torque ripple compensation. Fig. 2 shows the function of this current controller. The input is current command I_{tot}^* dependent on BLDC operating conditions while the output is desired DC voltage command V_{DC}^* for voltage controller.

The proposed current control consists of both feedback control and feedforward control. For the feedback control, the current controller is formulated by both proportional and integral (PI) control. The corresponding PI controller $G_{cc}(s)$ is designed by (4).

$$G_{cc}(s) = K_{i_P} + \frac{K_{i_I}}{s} K_{i_P} = 2BW_I \cdot L_s K_{i_I} = 2BW_I \cdot R_e \tag{4}$$

where K_{i_P} and K_{i_I} are respectively the proportional and integral gain.

In order to improve the current control bandwidth, the feedforward control is added for this current control. The feedforward controller is designed as the inverse of system transfer function from voltage output to current input. (5) depicts this feedforward controller G_{FFC} .

$$G_{FFC}(s) = \frac{BW_{volt}}{s + BW_{volt}} (2L_s s + 2R_e) \tag{5}$$

It is noted that a low pass filter with the same bandwidth BW as the proposed voltage controller is added to prevent unstable system because the upper bandwidth is limited by

the voltage control. For motion control applications with speed closed-loop, additional speed controller can be implemented. Similar to the current controller, a speed controller can be realized for the proposed BLDC drive.

IV. TORQUE RIPPLE COMPENSATION PROCESS

This section aims to compensate the torque ripple caused by the freewheeling current during diode conduction. The torque reduction from the freewheeling current is investigated. The DC voltage is regulated to maintain the torque output during diode conduction.

A. FREEWHEELING CURRENT REDUCTION

In addition to the DC-link current reduction and terminal voltage spike in Fig. 4, the freewheeling current also leads to the motor phase current variation. Because the motor current must be continuous during all BLDC commutation states, the energy stored in phase windings need to be released. According to Fig. 5, a single BLDC commutation consists of (a) diode conduction and (b) normal commutation. Considering the diode conduction in Fig. 5(a), corresponding motor three-phase currents can be derived through the equivalent circuit analysis. It is shown by (6)

$$\begin{aligned} I_{A_d} &= -I_0 e^{-(R_s/L_s)t} + \frac{V_{DC}/3 - E_A}{R_s} (1 - e^{-(R_s/L_s)t}) \\ I_{B_d} &= \frac{E_A + E_C - 2V_{DC}/3}{R_s} (1 - e^{-(R_s/L_s)t}) \\ I_{C_d} &= I_0 e^{-(R_s/L_s)t} + \frac{V_{DC}/3 - E_C}{R_s} (1 - e^{-(R_s/L_s)t}) \end{aligned} \tag{6}$$

when $t_0 < t < t_{xA}$ during V6 cycle in Fig. 5 (a) (6)

where I_0 is the initial condition of I_{tot} when diode conduction begins in Fig. 4(b), R_s and L_s are respectively motor phase resistance and inductance, and E_A , E_B and E_C are corresponding three-phase EMF phase voltages at t_0 .

It is important that the freewheeling current I_{A_d} flows from motor A-phase to inverter, as seen in Fig. 5(a). By contrast for normal BLDC commutation in Fig. 5(b), motor phase currents are represented by (7)

$$\begin{aligned} I_A &= 0 \\ I_C &= -I_B \\ &= I_1 e^{-(t-t_{xA})R_s/L_s} + \frac{V_{DC}}{2R_s} (1 - e^{-(t-t_{xA})R_s/L_s}) \\ &\quad - \frac{E_B - E_C}{2R_s} (1 - e^{-(t-t_{xA})R_s/L_s}) \end{aligned} \tag{7}$$

when $t_0 + t_{xA} < t < t_1$ during V6 cycle in Fig. 5 (b)

where t_0 is the time when commutation stage V6 begins and t_1 is the time when commutation stage V6 is finished. I_1 in Fig. 4(b) is the initial condition when normal commutation begins. Equations (6) and (7) derives three-phase currents for the BLDC commutation in Fig. 5(a) and (b). In this state, the total current I_{tot} is equal to C-phase current I_C . Because the torque output is proportional to the total current I_{tot} , the

torque reduction can be evaluated by comparing C-phase current between (6) and (7). Assuming V_{DC} remains constant during both diode conduction and normal commutation, it can be derived I_{C_d} is smaller than I_C . It results in the torque reduction during diode conduction.

It is noted that the length of diode conduction period is dependent on the diode conduction time t_{xA} , which is derived by

$$t_{xA} = -\frac{L_s}{R_s} \ln\left(\frac{V_{DC}/3 - E_A}{R_s I_0 + V_{DC}/3 - E_A}\right) \quad (8)$$

As seen in (8), t_{xA} is dependent on the motor electric time constant L_s/R_s and DC voltage V_{DC} . Finally, the diode conduction is induced two times per phase every electric cycle, as demonstrated from the phase voltage in Fig. 4(a). Considering the influence of diode conduction, a torque ripple with 6th-order periodic harmonic per electric cycle is expected.

B. DIODE CONDUCTION COMPENSATION

This part proposes the DC voltage feedforward compensation to remove torque ripple caused by diode conduction. During the diode conduction, the torque output is decreased due to freewheeling current. In order to compensate this effect, V_{DC} command must be adjusted during conduction period. In order to realize the voltage compensation, three-phase diode conduction times $t_{xA}/t_{xB}/t_{xC}$ must be calculated first. Based on (8), $t_{xA}/t_{xB}/t_{xC}$ can be estimated by

$$\begin{aligned} \hat{t}_{xA} &= -\frac{\hat{L}_s}{R_s} \ln\left(\frac{V_{DC}/3 - \hat{E}_A}{\hat{R}_s I_{tot} + V_{DC}/3 - \hat{E}_A}\right) \\ \hat{t}_{xA} &= \hat{t}_{xB} = \hat{t}_{xC} = \hat{t}_x \end{aligned} \quad (9)$$

In (9), a three-phase balanced motor is assumed where the conduction times among three-phase should be all the same as Besides, the estimated A-phase EMF \hat{E}_A in (9) can be obtained by (10). Assuming a balanced three-phase motor, the magnitude of three-phase EMF should have the same magnitude $|E|$ for six-step BLDC commutation.

$$\begin{aligned} \hat{E}_A &= (V_{DC} - -2\hat{R}_s I_{tot} - 2\hat{L}_s \frac{dI_{tot}}{dt})/2 \\ \hat{E}_A &= \hat{E}_B = -\hat{E}_C = |\hat{E}| \end{aligned} \quad (10)$$

Similar to (9), three-phase EMF voltages at the time instant t_0 is assumed the same with balanced windings. To maintain the constant torque during diode conduction, the current controller output V_{DC}^* form Fig. 2 can be modified by $V_{DC_com}^*$ in (11). Taking A-phase diode conduction in Fig. 5 for example, the phase current flows across A-phase resistance and EMF voltage should be compensated. By contrast, the DC voltage decreases to original V_{DC}^* once the drive leaves from diode conduction to normal commutation. Under this effect, the overall DC voltage compensation is proposed by

$$\begin{aligned} V_{DC_com}^* &= V_{DC}^* + \hat{R}_s I_{tot} + \hat{E}, \text{ when } t_0 < t < t_{xA} \\ V_{DC_com}^* &= V_{DC}^*, \text{ when } t_0 + t_{xA} < t < t_1 \end{aligned} \quad (11)$$

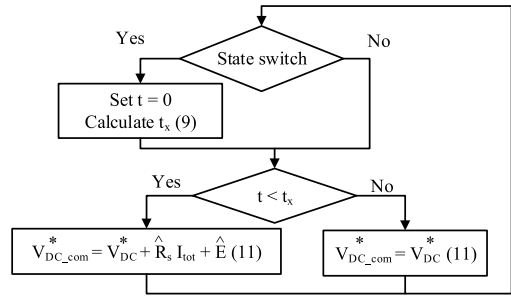


FIGURE 6. Flowchart of diode conduction ripple compensation process.

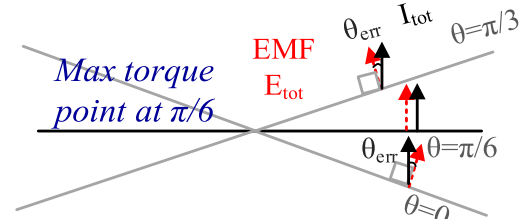


FIGURE 7. Vector relationship of EMF and BLDC regulated current with respect to rotor position during sector V1 in Fig. 5 (peak torque at $\pi/6$).

where t_0 and t_1 are the same as (6) and (7). In (11), the voltage drop due to inductance L_s is not taken into consideration due to voltage controller response limitation. Fig. 6 shows the signal flowchart of the proposed torque ripple compensation. It is noted that this process is executed once the BLDC commutation is changed during every six-step commutation.

C. BLDC CURRENT VECTOR ADJUSTMENT

In addition to the diode freewheeling current, the unchanged BLDC controlled current vector during every commutation stage also reduces the torque output. On the basis, the torque output of BLDC motor drive can be derived by

$$T_{em} = (I_A \times E_A + I_B \times E_B + I_C \times E_C)/\omega_m \quad (12)$$

where T_{em} is electromagnetic torque and ω_m is motor mechanical speed. In (12), the peak T_{em} is happened once the current vector is aligned with EMF voltage vector.

Fig. 7 shows the vector diagram relationship of the flux, EMF and BLDC regulated current vector at different rotor positions. The peak torque appears when the EMF and current vector are aligned with each other at the position of $\pi/6$ during sector V1 in Fig. 5. However for other positions, the current vector deviation occurs leading to torque T_{em} variation. It is important that the DC voltage can be regulated with respect to rotor position to improve this misalignment reflected torque ripple. For every BLDC commutation, the corresponding T_{em} can be derived by (13) through (12). It is given by

$$\begin{aligned} T_{em} &= (I_{C_d} \times E_C - I_{DC} \times E_B + I_{DC} \times E_A)/\omega_m \\ &= \vec{I}_{tot} \cdot \vec{E}_{tot}/\omega_m \\ &= |\vec{I}_{tot}| \times |\vec{E}_1| + |\vec{E}_3| \times \cos(\theta_{err})/\omega_m \end{aligned} \quad (13)$$

where \vec{I}_{tot} is the synthesized current vector. Considering the operation under sector V1, \vec{I}_{tot} is the black solid vector in

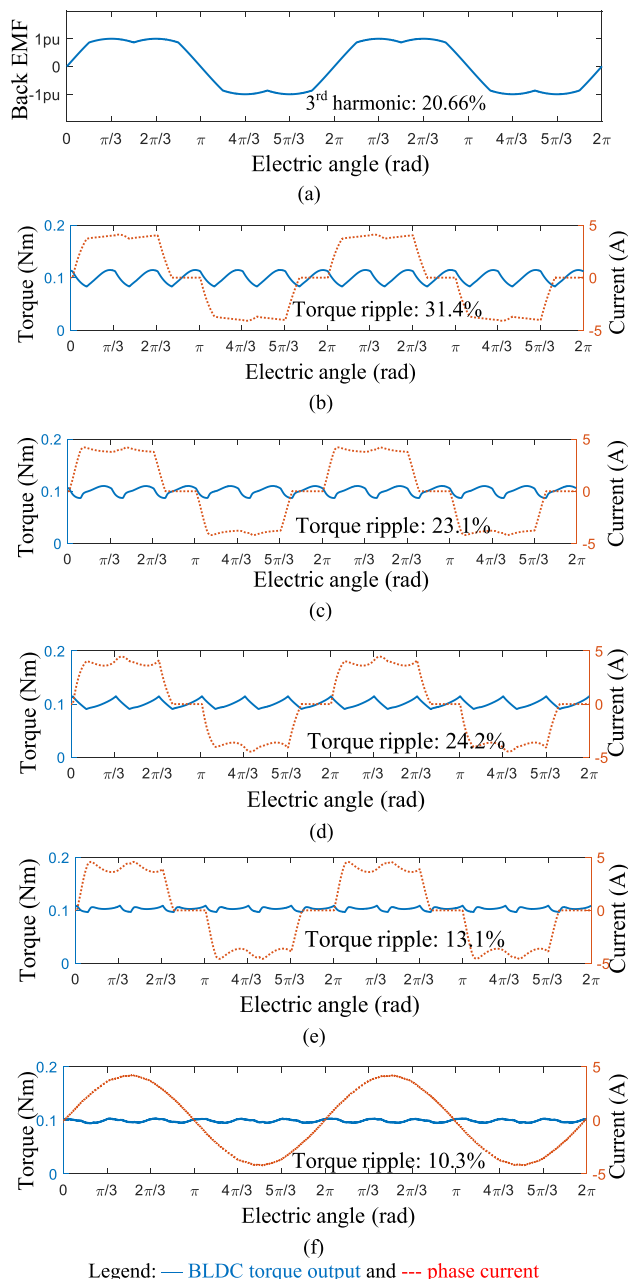
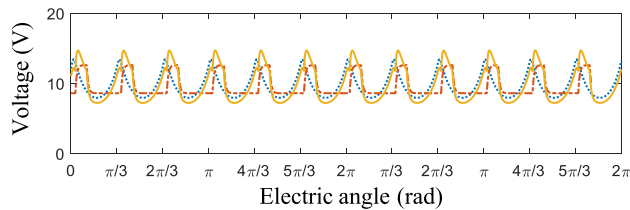


FIGURE 9. Phase current and torque simulation result on a PM motor with sinusoidal EMF: (a) the corresponding EMF, (b) normal BLDC drive, (c) BLDC drive with diode compensation, (d) BLDC with current adjustment, (e) both diode compensation and current adjustment, (f) SVPWM FOC drive (1000rpm and 0.1Nm rated torque).

EMF waveform contains a 20.66% 3rd-order EMF harmonic due to the saturation. Fig. 9(b) shows both the torque output and A-phase current without the torque ripple compensation.

$$\begin{aligned}
 I_{tot}^* &= (I_{tot1}^* \times I_{tot2}^*) / I^* \\
 &= \frac{1}{\cos(\hat{\theta}_e - \pi/6)[\cos(\hat{\theta}_e - \pi/6 - \varphi) + R_{31}\cos 3(\hat{\theta}_e - \pi/6 - \varphi)]} \\
 &\text{when } 0 < \hat{\theta}_e < \pi/3
 \end{aligned}
 \tag{18}$$



Legend: --- Diode compensation, ... Current adjustment and — Diode compensation and current adjustment

FIGURE 10. Comparison of DC voltage control among different torque ripple compensation method.

The peak-to-peak torque ripple is around 31.4%. In this paper, following torque ripples are all calculated by peak-to-peak values. The phase current is distorted from the ideal trapezoidal waveform with periodic 6th-order harmonic. By contrast, Fig. 9(c) shows the same torque and current waveform when the proposed diode conduction compensation in Fig. 6 is added. The torque ripple is reduced from 31.4% to 23.1% while the trapezoidal phase current distortion still appears.

Fig. 9(d) further illustrates the torque and current when the proposed current vector adjustment in (18) is applied. In this case, the torque ripple is improved from 31.4% to 24.2%. It is observed that both the diode conduction and current vector misalignment results in the similar ripple effect on BLDC drives. Consequently, Fig 9(e) demonstrates the BLDC drive combining both ripple compensation methods in Fig. 8. The resulting torque ripple reduces to 13.1%. More importantly, the phase current is close to the six-step trapezoidal current where the magnitude is larger respectively at the beginning and ending of each conduction sub-period. Finally, Fig. 9(f) compares the torque ripple for the sinusoidal EMF motor with SVPWM FOC drive using 1kHz bandwidth current control and 10kHz switching frequency. The torque ripple is 10.3% caused by motor EMF harmonics and PWM switching. For the PM motor with sinusoidal EMF, it is concluded that the proposed BLDC drive reduces around 18% torque ripple although the ripple is 2.8% slightly higher than FOC drive.

Fig. 10 compares the DC voltage control performance under different torque ripple compensation methods. Considering only the diode conduction compensation, DC voltage has a step level change during conduction period, shown as red dash line. By contrast for the current adjustment, the DC voltage is manipulated dependent on the current controller. In this case, the DC voltage is changed with respect to different rotor positions. By combining these two ripple

TABLE 4. Simulation motor characteristics.

Motor characteristics	Values
Rotor poles	12 poles
Rated power	4.08kW
Rated torque	6.5 Nm
Rated speed	6krpm (628.32 rad/s)
Motor resistance	0.013Ω
Motor inductance	0.22mH

compensation methods, the resulting DC voltage is a mixed signal of previous two voltages, as shown by the orange solid line. It is also noted that this compensated voltage results in a 6th-order periodic harmonic. The 6th-order torque harmonic in Fig. 9 is decreased based on this 6th-order voltage harmonic regulation.

B. PM MOTOR WITH TRAPEZOIDAL EMF

To show the proposed method works on different motors, a PM motor with trapezoidal EMF is also used for simulation. Table 4 lists corresponding motor characteristics. The rated torque is 6.5Nm with 6krpm rated speed. Due to the motor availability and bench limitation, this trapezoidal EMF motor is only verified through simulation. Nevertheless, the ripple compensation on different motor types can still be compared.

Fig. 11(a) illustrates the corresponding phase EMF waveform for this trapezoidal PM motor. Similar to the sinusoidal motor simulation in Fig. 9, five different conditions are compared. They are 1) normal BLDC drive without compensation, 2) BLDC drive with proposed diode compensation, 3) BLDC with proposed current adjustment, 4) both diode compensation and current adjustment and 5) SVPWM FOC drive.

Fig. 11(b) shows the torque and A-phase current without the torque ripple compensation. Torque ripple is around 27.0%. Comparing to the sinusoidal EMF motor in Fig. 9(b), the torque ripple is slightly lower through BLDC six-step commutation. By contrast, Fig. 11 (c) shows the same torque and current when the diode compensation is implemented. The ripple is improved from 27.0% to 20.2%. Similar to diode compensation, the comparable ripple compensation with 21.5% is achieved using the proposed current adjustment as seen in Fig. 11(d).

Once both compensation methods are applied, the torque ripple is minimized to 13.6% in (e). Comparing the sinusoidal motor in Fig. 9 and trapezoidal motor in Fig. 11, the similar torque ripple performance is concluded after the proposed compensation. However, for sinusoidal EMF motor, almost 18% of torque ripple is reduced. This improvement is better than the use on trapezoidal motor with only 13% reduction performance. Finally, Fig. 11(f) simulates the torque ripple for the trapezoidal EMF motor using SVPWM FOC drive under the same control bandwidth and switching frequency. It is concluded that for the proposed PAM BLDC drive, the torque ripple can be lower than SVPWM drive for trapezoidal EMF motors.

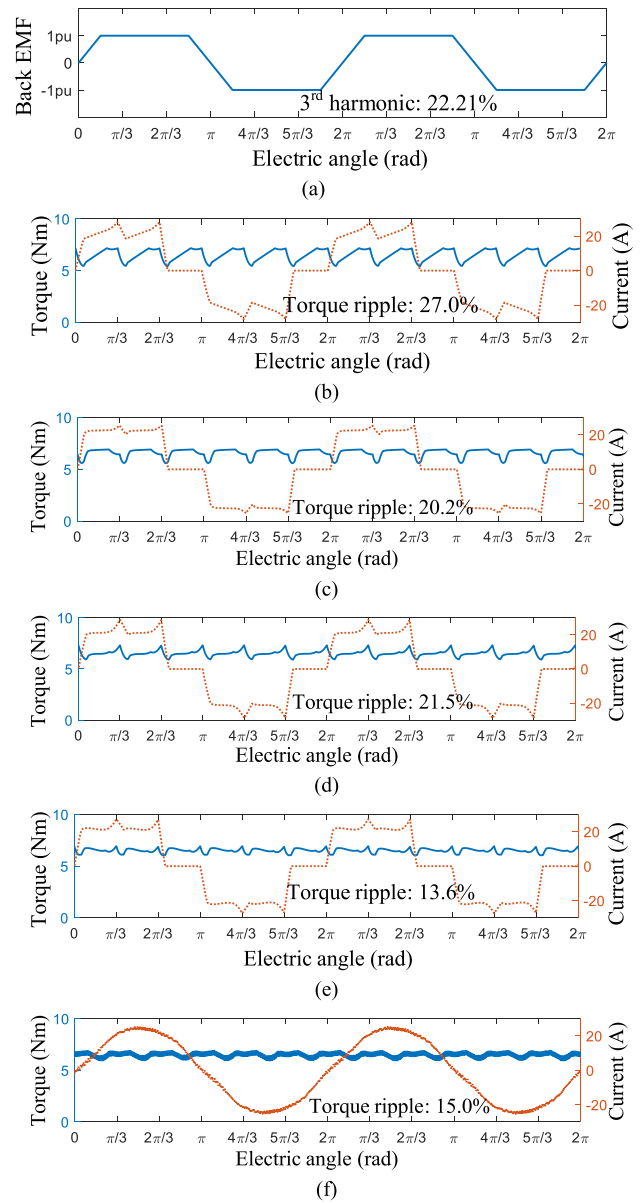


FIGURE 11. Phase current and torque simulation result using a trapezoidal wave back EMF motor: (a) the corresponding EMF, (b) normal BLDC drive, (c) BLDC drive with diode compensation, (d) BLDC with current adjustment, (e) both diode compensation and current adjustment, (f) SVPWM FOC drive (1000rpm and 0.1Nm rated torque).

VI. EXPERIMENTAL RESULTS

The same sinusoidal PM motor in Table 2 is used for the experimental evaluation of proposed BLDC torque ripple compensation. Motor and inverter parameters are the same as simulation in section IV. For the front-end DC converter in Fig. 1, the PWM frequency is at 500kHz for the LC filter volume minimization. Experiment platform uses a DC voltage supply as power source; however, battery is also suitable for the proposed method since the maximum supply current ripple does no increase much. The voltage and current sample frequency is 100kHz synchronous to interrupt service routine.

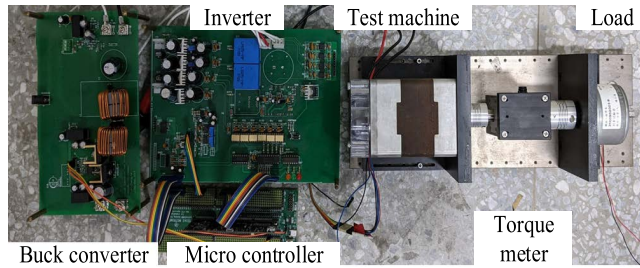


FIGURE 12. Experimental setup of PAM drive system.

Fig. 12 illustrates the proposed BLDC drive test setup. A hysteresis load is coupled with the motor for the load operation. It is noted that the couple between hysteresis load and drive system might induce additional torque ripples. Consequently, experiment torque ripple is larger than simulation. All torque ripple compensation methods are implemented in a 200MHz microcontroller, TI-TMS320F28379D.

A. DC BUS VOLTAGE AND CURRENT CONTROL VERIFICATION

This part verifies the proposed voltage and current control for the PAM voltage modulation in section III. Considering the diode conduction current compensation in Fig. 6, the proposed torque ripple compensation relies on the high dynamic DC voltage modulation.

In order to verify the dynamic DC voltage modulation, the test motor is locked at zero speed to clearly evaluate the proposed controller in section III. Fig. 13(a) shows the voltage regulation using the proposed voltage control in (3). For the voltage command V_{DC}^* , a 2V DC voltage with 1V AC harmonic at 1kHz is directly manipulated to show the voltage controller capability. It is shown that the proposed voltage control with the filter resonant compensation can achieve 1kHz voltage tracking with negligible magnitude drop and phase delay. The proposed voltage controller demonstrates 1kHz DC voltage harmonic modulation to be compatible with the diode reflected torque ripple compensation.

Fig. 13(b) further illustrates the current control performance. As seen in Fig. 7, the torque ripple compensation based on the current vector adjustment requires a high bandwidth DC current manipulation. In this test, a 0.4A DC current I_{tot}^* with 0.2A AC harmonic at 500Hz is given. It is shown that the proposed current control can also achieve around 500Hz bandwidth for the implementation of current vector adjustment.

B. TORQUE RIPPLE REDUCTION AT LOW SPEED

This part verifies the proposed torque ripple reduction in section IV. It is noteworthy that the DC current controller bandwidth is designed at 500Hz. Considering the voltage modulation of 6th-order harmonic with respect to rotor frequency in Fig. 10, the maximum operating frequency is around $500/6=83.3$ Hz. Nevertheless at high speed, the torque ripple decreases dramatically. It will be verified at part D

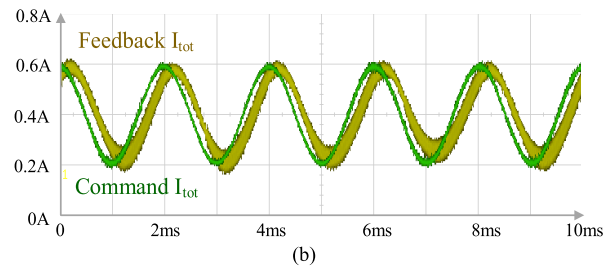
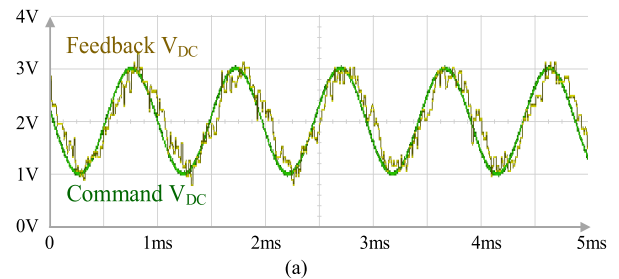


FIGURE 13. Proposed DC-link voltage and current control performance: (a) 2V DC voltage with 1V AC harmonic at 1kHz and (b) 0.4A DC current with 0.2A AC harmonic at 500Hz (100 kHz controller sampling frequency).

in this section. More importantly, the current control bandwidth can be increased by increasing the converter PWM frequency.

Fig. 14 compares the BLDC drive before and after the proposed torque ripple compensation. In this experiment, the motor is speed controlled to maintain at 66.6Hz (1000 rpm) under load. The torque output is measured from the torque meter illustrated in Fig. 12. The overall BLDC control process is shown in Fig. 2. As seen for normal BLDC drive in Fig. 14(a), the trapezoidal phase current is distorted during each BLDC commutation. The peak-to-peak torque ripple is 81.3% containing a visible 6th-order harmonic. Comparing to simulation in Fig. 10, the experiment result shows the higher torque ripple. The mechanical strength of test bench, rotating shaft misalignment and torque harmonics from hysteresis brake all cause additional torque ripples.

Fig. 14(b) shows the BLDC drive after the proposed diode conduction compensation in Fig. 6. The test condition is the same as Fig. 14(a). Similar to simulation in Fig. 9, DC voltage contains the similar step level change. Although phase current is still not a normal trapezoidal wave, torque ripple can be reduced to 52.5% after compensating diode reflected ripple component.

Fig. 14(c) shows the BLDC drive after another proposed current vector adjustment in (19). By manipulating DC current dependent on the rotor position, phase current can be similar to trapezoidal current simulated in Fig. 9(c). Consequently, torque ripple is reduced to 62.5% where the DC voltage contains 6th-order periodic harmonic.

Finally, Fig. 14(d) shows the BLDC drive after both ripple compensation methods. Modulated DC voltage is the combination of step change in (b) and 6th-order harmonic in (c). In addition, phase current is close to ideal trapezoidal current with peak magnitude respectively at the beginning

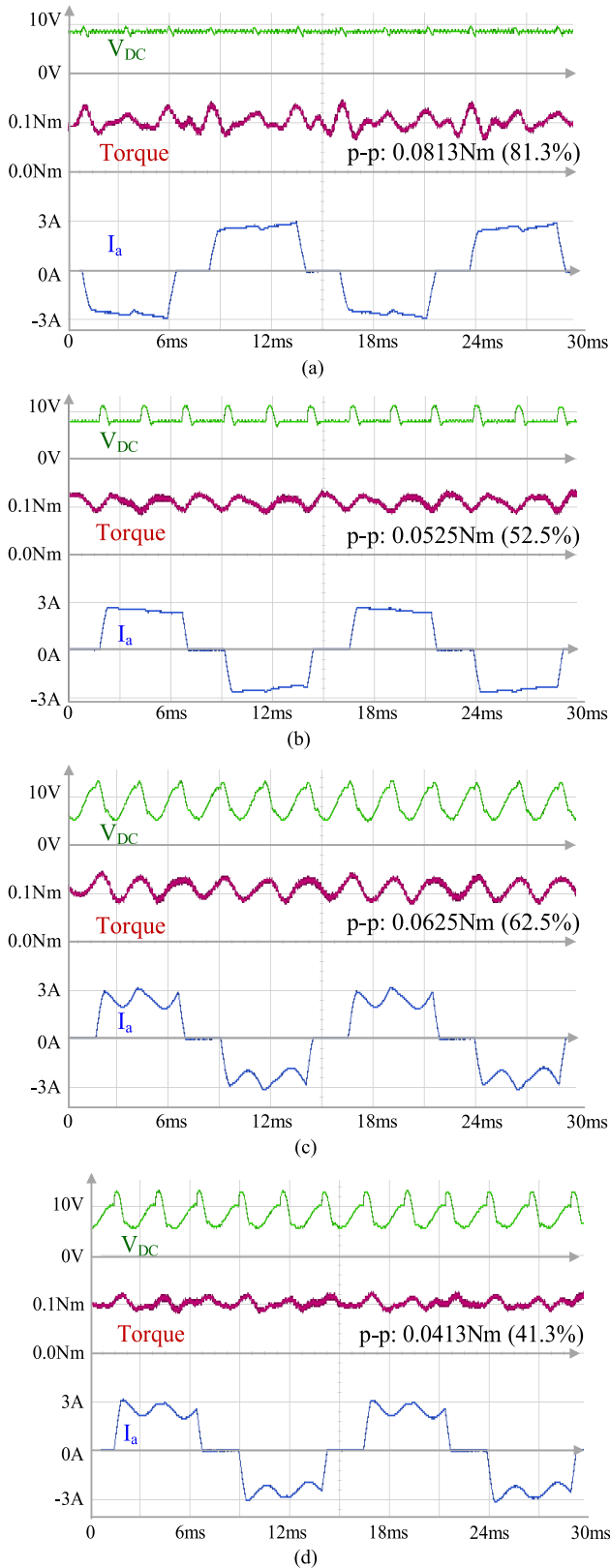


FIGURE 14. Torque ripple comparison for BLDC drive at 66.67Hz rotor frequency (1000rpm speed): (a) normal drive, (b) drive with diode compensation, (c) current adjustment and (d) both diode compensation and current adjustment (full load and speed closed-loop).

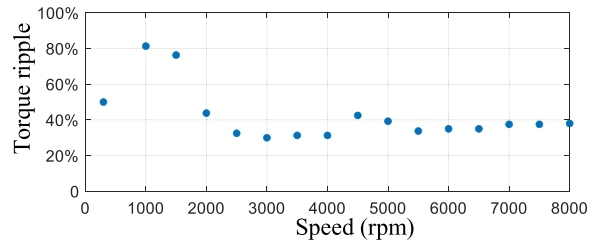


FIGURE 15. Relation between torque ripple and motor speed with no compensation method.

and ending of each commutation. In this case, the torque ripple is improved from normal 81.3% to 41.3% with around 40% ripple improvement. The experiment results in Fig. 14 is consistent with the simulation in Fig. 9. The commutation issues caused by diode conduction and current vector misalignment lead to a similar ripple effect on BLDC drives. The proposed compensation combined with front-end DC voltage modulation can effectively reduce these two BLDC torque ripple components.

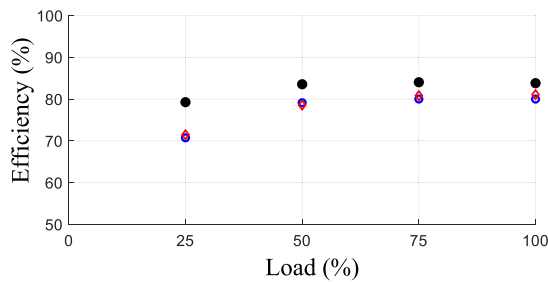
C. TORQUE RIPPLE AT HIGH SPEED

It is noted that the proposed ripple compensation is based on the high bandwidth DC voltage modulation. It results in the limitation at high speed with high rotor operating frequency. Nevertheless, the BLDC torque ripple is reduced as speed increases.

Considering the diode conduction ripple, the conduction time t_{xA} in (9) is decreased as the increase of EMF voltage EA. Under this effect, the diode conduction ripple is inversely proportional to the motor speed, as also reported in [20]. Fig. 15 demonstrates the corresponding torque ripple as speed increases for normal BLDC drive, speed over 8000rpm can cause the mechanical system unstable. It is shown that the torque ripple starts to decrease when the conduction time t_x is smaller than a certain value over 1500rpm motor speed. The torque ripple is slightly increased at 4500rpm due to the mechanical resonance. Based on this experiment, it is concluded that the BLDC reflected torque ripple is relatively high at low speed which can be compensated by the proposed ripple compensation.

D. PAM BLDC EFFICIENCY

This part evaluates the BLDC drive efficiency using the proposed torque ripple compensation. Fig. 16 compares the motor efficiency among the proposed PAM BLDC drive, conventional BLDC and SVPWM FOC. Similar to Fig. 14, the motor speed is controlled to maintain at 1000rpm. In this experiment, the proposed BLDC drive shows the best efficiency while the conventional BLDC results in the worst efficiency. Because of PAM voltage control, the motor iron loss can be minimized. Instead of torque ripple reduction, it is important that the efficiency improvement is another



Legend: ● proposed PAM BLDC, ● conventional PWM BLDC and ◊ SVPWM FOC

FIGURE 16. Motor efficiency comparison among proposed PAM BLDC drive, conventional PWM BLDC and SVPWM FOC under 1000rpm.

benefit for the proposed BLDC with DC voltage regulation. The same efficiency improvement comparing to SVPWM is also reported in [10].

VII. CONCLUSION

This paper proposes a torque ripple compensation for BLDC drives with six-step commutation. A front-end DC converter is developed to achieve the high-bandwidth DC-link voltage and current modulation. The torque ripple caused by the diode freewheeling current and current vector misalignment are compensated with the DC voltage and current control. Both the simulation and experiment verify the torque ripple compensation performance. According to experimental results, around 40% torque ripple is improved using the proposed PAM BLDC drive. The proposed method is applicable for low speed operation including start-up.

REFERENCES

- [1] T. M. Jahns and W. L. Soong, "Pulsating torque minimization techniques for permanent magnet AC motor drives—A review," *IEEE Trans. Ind. Electron.*, vol. 43, no. 2, pp. 321–330, Apr. 1996.
- [2] H. Lu, L. Zhang, and W. Qu, "A new torque control method for torque ripple minimization of BLDC motors with un-ideal back EMF," *IEEE Trans. Power Electron.*, vol. 23, no. 2, pp. 950–958, Mar. 2008.
- [3] J. H. Song and I. Choy, "Commutation torque ripple reduction in brushless DC motor drives using a single DC current sensor," *IEEE Trans. Power Electron.*, vol. 19, no. 2, pp. 312–319, Mar. 2004.
- [4] J. Fang, H. Li, and B. Han, "Torque ripple reduction in BLDC torque motor with nonideal back EMF," *IEEE Trans. Power Electron.*, vol. 27, no. 11, pp. 4630–4637, Nov. 2012.
- [5] D.-K. Kim, K.-W. Lee, and B.-I. Kwon, "Commutation torque ripple reduction in a position sensorless brushless DC motor drive," *IEEE Trans. Power Electron.*, vol. 21, no. 6, pp. 1762–1768, Nov. 2006.
- [6] H. K. S. Ransara and U. K. Madawala, "A torque ripple compensation technique for a low-cost brushless DC motor drive," *IEEE Trans. Ind. Electron.*, vol. 62, no. 10, pp. 6171–6182, Oct. 2015.
- [7] W. Jiang, P. Wang, Y. Ni, J. Wang, L. Wang, and Y. Liao, "Multimode current hysteresis control for brushless DC motor in motor and generator state with commutation torque ripple reduction," *IEEE Trans. Ind. Electron.*, vol. 65, no. 4, pp. 2975–2985, Apr. 2018.
- [8] G. Buja, M. Bertoluzzo, and R. K. Keshri, "Torque ripple-free operation of PM BLDC drives with petal-wave current supply," *IEEE Trans. Ind. Electron.*, vol. 62, no. 7, pp. 4034–4043, Jul. 2015.
- [9] Y.-S. Lai, K.-Y. Lee, J.-H. Tseng, Y.-C. Chen, and T.-L. Hsiao, "Efficiency comparison of PWM-controlled and PAM-controlled sensorless BLDCM drives for refrigerator applications," in *Proc. IEEE Ind. Appl. Annu. Meeting*, Sep. 2007, pp. 268–273.

- [10] L. Schwager, A. Tuysuz, C. Zwyssig, and J. W. Kolar, "Modeling and comparison of machine and converter losses for PWM and PAM in high-speed drives," *IEEE Trans. Ind. Appl.*, vol. 50, no. 2, pp. 995–1006, Mar. 2014.
- [11] K.-Y. Nam, W.-T. Lee, C.-M. Lee, and J.-P. Hong, "Reducing torque ripple of brushless DC motor by varying input voltage," *IEEE Trans. Magn.*, vol. 42, no. 4, pp. 1307–1310, Apr. 2006.
- [12] T. Shi, Y. Guo, P. Song, and C. Xia, "A new approach of minimizing commutation torque ripple for brushless DC motor based on DC-DC converter," *IEEE Trans. Ind. Electron.*, vol. 57, no. 10, pp. 3483–3490, Oct. 2010.
- [13] G. D. Marques and M. F. Iacchetti, "Minimization of torque ripple in the DFIG-DC system via predictive delay compensation," *IEEE Trans. Ind. Electron.*, vol. 65, no. 1, pp. 103–113, Jan. 2018.
- [14] S. J. Park, H. W. Park, M. H. Lee, and F. Harashima, "A new approach for minimum-torque-ripple maximum-efficiency control of BLDC motor," *IEEE Trans. Ind. Electron.*, vol. 47, no. 1, pp. 109–114, Feb. 2000.
- [15] M. Antivachis, J. A. Anderson, D. Bortis, and J. W. Kolar, "Analysis of a synergetically controlled two-stage three-phase DC/AC buck-boost converter," *CPSS Trans. Power Electron. Appl.*, vol. 5, no. 1, pp. 34–53, Mar. 2020.
- [16] C.-L. Huang, C.-J. Wu, and S.-C. Yang, "Full-region sensorless BLDC drive for permanent magnet motor using pulse amplitude modulation with DC current sensing," *IEEE Trans. Ind. Electron.*, vol. 68, no. 11, pp. 11234–11244, Nov. 2021.
- [17] T.-F. Wu and Y.-K. Chen, "Modeling PWM DC/DC converters out of basic converter units," *IEEE Trans. Power Electron.*, vol. 13, no. 5, pp. 870–881, Sep. 1998.
- [18] C. Zwyssig, J. W. Kolar, and S. D. Round, "Megaspeed drive systems: Pushing beyond 1 million r/min," *IEEE/ASME Trans. Mechatronics*, vol. 14, no. 5, pp. 564–574, Oct. 2009.
- [19] F. G. Capponi, G. D. Donato, L. D. Ferraro, O. Honorati, M. C. Harke, and R. D. Lorenz, "AC brushless drive with low-resolution Hall-effect sensors for surface-mounted PM machines," *IEEE Trans. Ind. Appl.*, vol. 42, no. 2, pp. 526–535, Mar. 2006.
- [20] H.-Y.-O. Yang and R. D. Lorenz, "Torque ripple minimization in six-step PMSM drives via variable and fast DC bus dynamics," *IEEE Trans. Ind. Appl.*, vol. 55, no. 4, pp. 3791–3802, Jul. 2019.



CHING-LON HUANG (Student Member, IEEE) was born in Taiwan. He received the B.S. degree in mechanical engineering from the National Taiwan University, Taipei, Taiwan, in 2018, where he is currently pursuing the Ph.D. degree in mechanical engineering. His current research interests include servo motor systems, transport drone motor control, traction motor, and high-speed motor drive systems.



FENG-CHI LEE received the B.S. degree in mechanical control engineering from the National Taiwan University of Science and Technology, Taipei, Taiwan, in 2005, and the M.S. degree in mechanical control engineering from the National Taipei University of Technology, Taipei, in 2007. He is currently working with the Industrial Technology Research Institute, with the responsibility on the development of electromechanical control technology. His research interests include motion control, machine vision, and electromechanical systems.

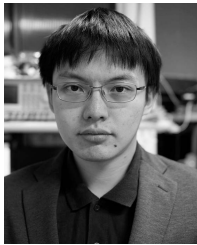


include motion control, automatic control, and electromechanical systems.

CHIA-JUNG LIU received the B.S. degree in mechanical engineering from the National Kaohsiung First University of Science and Technology, Kaohsiung, Taiwan, in 2010, and the M.S. degree in mechanical engineering from the National Taiwan University of Science and Technology, Taipei, Taiwan, in 2012. He is currently working with the Industrial Technology Research Institute, with the responsibility on the development of electromechanical control technology. His research interests



YI-JEN LIN (Graduate Student Member, IEEE) was born in Taiwan. He received the B.S. degree in mechanical engineering from the National Taipei University of Technology, Taipei, Taiwan, in 2019. He is currently pursuing the Ph.D. degree in mechanical engineering with the National Taiwan University, Taipei. His current research interests include motor drive systems and high-precision motion control systems.



JYUN-YOU CHEN (Student Member, IEEE) was born in Taichung, Taiwan, in 1992. He received the B.S. degree in communication engineering from Feng Chia University, Taichung, in 2015, and the M.S. degree in mechanical engineering from the National Central University, Taoyuan, Taiwan, in 2017. He is currently pursuing the Ph.D. degree and dissertator in mechanical engineering with the National Taiwan University, Taipei, Taiwan. His research interests include motor drive and control systems.



SHIH-CHIN YANG (Senior Member, IEEE) was born in Taiwan. He received the M.S. degree from the National Taiwan University, Taiwan, in 2007, and the Ph.D. degree from the University of Wisconsin–Madison, Madison, WI, USA, in 2011. From 2011 to 2015, he was a Research Engineer with Texas Instruments Motor Laboratory, Dallas, TX, USA. He is currently a Professor with the National Taiwan University, with the responsibility on the development of motor drive and motor control technology. His research interests include motor drive, power electronics, and control systems. He was a recipient of the IEEE Industry Applications Society Industrial Drive Committee First Prize Paper Award in 2011.

...